Cloud Clusters and Large-Scale Vertical Motions in the Tropics

By Robert A. Houze, Jr.

Department of Atmospheric Sciences, University of Washington
Seattle, Washington 98195, U.S.A.
(Manuscript received 1 October 1981)

Abstract

The sensible heat budget of a large-scale area containing an idealized tropical cloud cluster is analyzed. The cluster is assumed to have spatial dimensions and precipitation rates typical of observed cloud clusters.

In its early stages of development the idealized cluster consists of isolated deep precipitating convective cells, or "hot towers." A simple model using the assumed precipitation rates as input is employed to compute the condensation and evaporation rates and sensible heat fluxes associated with the precipitating hot towers. The condensation dominates the contribution of the hot towers to the large-scale heat budget, and the net effect of the towers is warming distributed through the full depth of the troposphere.

In its mature stage of development, the idealized cluster contains not only convective towers but a widespread cloud shield interconnecting the towers. The cloud shield is dynamically and thermodynamically active, and processes associated with it also contribute significantly to the large-scale sensible budget. Stratiform precipitation falls from the cloud shield, and in the stratiform precipitation region, condensation occurs in mesoscale updraft aloft, evaporation occurs in a mesoscale downdraft at low levels and melting occurs in a middle-level layer. The condensation, evaporation and sensible heat transports associated with the mesoscale updraft and downdraft are determined from simple models using the cluster's assumed stratiform precipitation rate as input. The evaporation and melting in the stratiform precipitation region are also estimated from vertical profiles of radar reflectivity in real cloud clusters. The total effects of the stratiform precipitation processes on the large-scale heat budget are warming of the middle to upper troposphere, where condensation in the mesoscale updraft is the dominant effect, and cooling in the lower troposphere, where melting and mesoscale downdraft evaporation dominate.

The widespread cloud shield present in the mature and later stages of a cloud cluster's life cycle is also an important absorber and emitter of radiation. Radiative transfer models applied to tropical cloud shields show substantial heating effects in the middle to upper troposphere. These effects are nearly as important as the heating by convective towers and the heating and cooling associated with the stratiform precipitation processes.

As the idealized cloud cluster progresses from early to mature stages of development, its net effect on the large-scale heat budget changes. As the cloud shield develops, the mesoscale updraft condensation and radiation reinforce the heating by convective towers aloft, while the mesoscale downdraft evaporation and melting counteract the convective-tower heating at low levels. Thus, the net heating by the cluster increases in the upper troposphere and decreases in the lower troposphere as the system develops. Large-scale upward motion, which is required to balance the large-scale heat budget against the effects of the cluster, is thus expected to increase aloft and decrease at low levels. Vertical motions deduced from large-scale wind observations in the tropics confirm this expectation. Thus, it is concluded that the mesoscale stratiform and radiative processes associated with the cloud shields of developing cloud clusters are sufficiently strong to alter the large-scale vertical motion field in the tropics.

1. Introduction

In the equatorial trough zone, cumulus-scale cloud towers, ranging from shallow trade wind cumulus to very deep "hot" towers, are important elements of the large-scale circulation (Riehl and Malkus, 1958; Riehl and Simpson, 1979). Yet, when viewed by satellite, the cloud pattern in

equatorial regions is more complex than that of an ensemble of towers only. In particular, the pattern is dominated by mesoscale shields of cirrus, each shield being ~100-1,000 km in horizontal dimension (*e.g.*, the cloud patches along 10°N in Fig. 1). In early satellite studies (Martin and Karst, 1969; Frank, 1970; Martin and Suomi, 1972), these cirrus shields were identified and called "cloud clusters", since hot towers appeared to be located preferentially within the regions of the cloud shields. For a long time, it was questioned whether the cirrus shields seen in satellite imagery represent a significant scale of motion or are inactive regions of inert upper-level cloud connecting the active convective towers. Data collected in field experiments in the tropics over the past 15 years, however, have consistently shown that the cloud shields seen by satellite are indeed active, with significant organization of air motions and thermodynamic processes on the 100-1,000 km scale (see review by Houze and Betts, 1981).

The typical life cycle and structure of a cloud cluster [adapted from studies by Leary and Houze (1979a, b, 1980), Webster and Stephens (1980) and Gamache and Houze (1982)] is illustrated schematically in Fig. 2. In its mature stage (Fig. 2b), the cluster consists partly of convective towers, which contain buoyant updrafts, negatively buoyant downdrafts and heavy showers of rain. In addition, lighter precipitation extends over a horizontal distance of 100-200 km. It falls from a deep stratiform cloud extending from the mid-troposphere to the top of the cirrus shield. Within the stratiform cloud is a mesoscale updraft of air rising at 10-50 cm s^{-1}. [The existence of the mesoscale updraft, uncertain until recently, has been shown definitively by Gamache and House (1982)]. Ice particles growing and drifting downward through the mesoscale updraft melt in a thin layer, well-defined as a bright band in radar observations, and evaporate partially as they fall as raindrops through an unsaturated mesoscale downdraft of the type described by Zipser (1969) below cloud base. The mesoscale updrafts and downdrafts are quite distinct from the convective drafts. They are widespread, gentle and hydrostatic, in contrast to the vigorous localized non-hydrostatic drafts of the convective towers. The mesoscale drafts, which have been

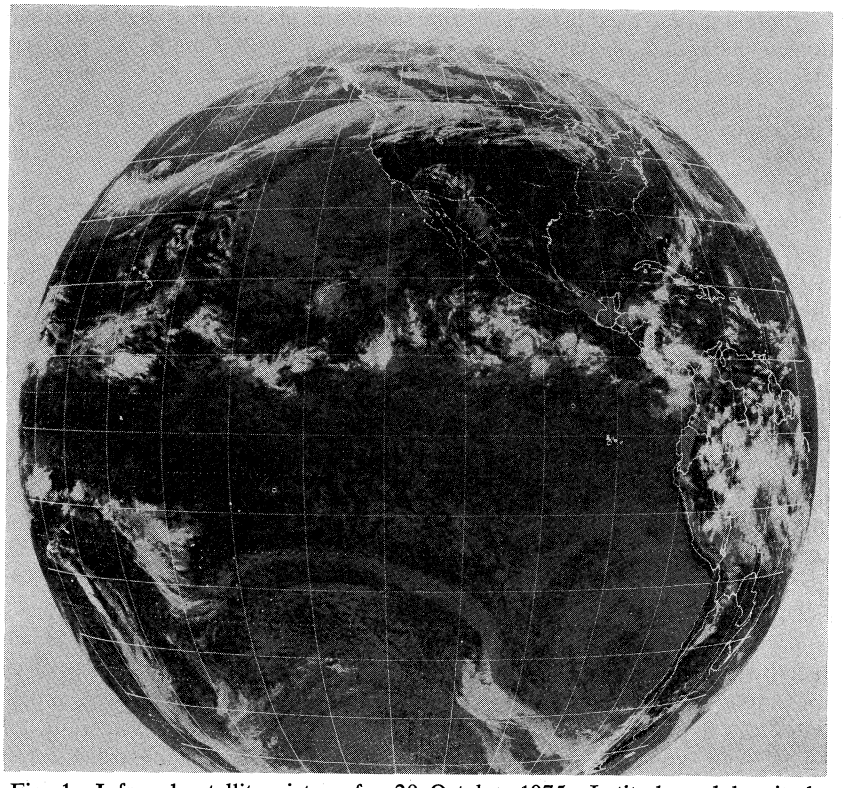

Fig. 1 Infrared satellite picture for 20 October 1975. Latitude and longitude interval is 5°.

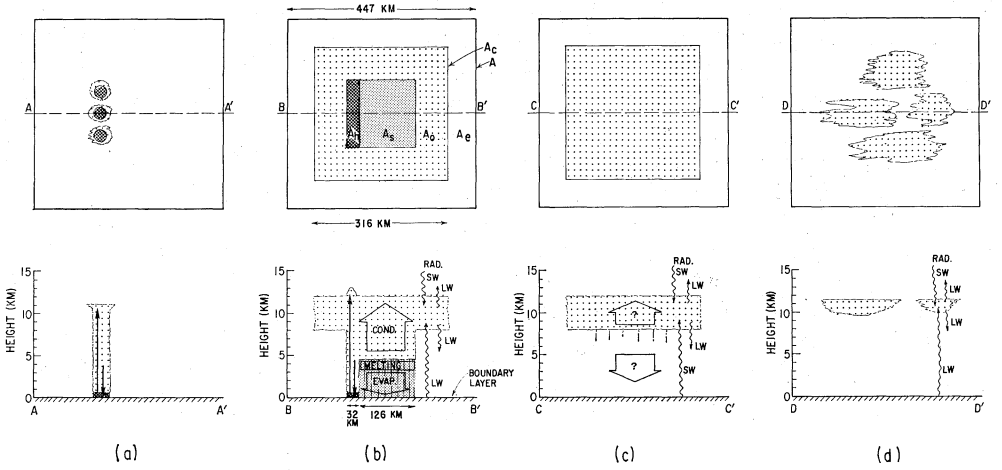

Fig. 2 Schematic of a tropical cloud cluster in four succcssive stages of development. (a) Early stage in which cluster consists of isolated precipitating convective towers. (b) Mature stage in which a cloud shield has developed and covers area A_c, convective cells ("hot towers") are located in area A_h, stratiform precipitation is falling from a middle-level cloud base within area A_s, and an area A_o is covered by upper-level cloud overhang. (c) Weakening stage in which convective cells have disappeared and stratiform precipitation is weak and not reaching the surface. (d) Dissipating stage in which no precipitation remains and upper cloud is becoming thin and breaking up. In (a) and (b), cumulus-scale updrafts and downdrafts are denoted by straight solid arrows. In (b) and (c), mesoscale updraft and downdraft are shown by wide, open arrows, and condensation (COND.) in the mesoscale updraft, evaporation (EVAP.) in the mesoscale downdraft and the melting layer in the stratiform precipitation region are indicated. Question marks indicate that the existence of the mesoscale drafts in stage (c) is uncertain. Short-wave (SW) and long-wave (LW) radiation (RAD.) are denoted by wavy arrows. The upper panels of (a)-(d) are plan views. The lower panels are vertical sections along the indicated horizontal line segments. Area A is a large-scale region containing the cloud cluster and A_e is a cloud-free environmental area surrounding the cluster.

both documented in case studies (*e.g.*, Gamache and Houze, 1982) and simulated in numerical models (*e.g.*, Brown, 1979), are fed by mid-level convergence in contrast to the boundary-layer convergence that feeds the updrafts of the convective towers.

When a cloud system attains the horizontal and vertical scale of a mature cloud cluster, radiative heating and cooling become significant. Therefore, solar and infrared absorption and emission are included schematically in Figs. 2b-d.

In various studies of cloud clusters that have been made as a result of tropical field experiments, particularly the Global Atmospheric Research Program's Atlantic Tropical (GATE) and Monsoon (MONEX) Experiments, the magnitudes of convective and mesoscale updrafts and downdrafts in clusters have been estimated, and the amounts of heating and cooling associated with condensation, evaporation, melting and radiation have been computed. However, these estimates and calculations appear in diverse papers and have not heretofore been brought together in a single assessment of the total thermodynamic effect of a tropical cloud cluster on a large-scale region containing it. In this paper, such an assessment is attempted by considering the sensible heat budget of a large-scale area containing the idealized cluster depicted in Fig. 2. From the cluster's net heating of the area, an understanding is obtained of how large-scale vertical motion in the tropics is related to the thermodynamic processes in cloud clusters. In particular, the separate roles of the convective towers, mesoscale stratiform precipitation processes and radiation in clusters in affecting large-scale motions are distinguished. The importance of the mesoscale stratiform processes and radiation thus revealed reflect the active rather than

passive nature of the cluster's cloud shield and indicate the necessity of taking mesoscale and radiative processes into account in considerations of large-scale motions in the tropics.

2. Properties of the idealized cloud cluster

To proceed with calculations, the idealized cloud cluster in Fig. 2 is assumed to have the same properties as the idealized cluster considered by Leary and Houze (1980, see their Fig. 1). These properties are listed in Table 1. The areas covered by convective or "hot" towers ($A_h=0.5\times 10^4$ km^2) and stratiform rain ($A_s=2.0\times 10^4$ km^2) are the same as in Leary and Houze's paper, although the lengths and widths of the features have been sketched slightly differently in Fig. 2 than in their paper. The area-integrated rainfall amounts in the convective and stratiform regions (1.5×10^{11} kg and 2.5×10^{11} kg for one hour, respectively) are also the same as in their paper. They worked with the total rainfall amounts over an 18 hour period, whereas in this paper the total rain for a representative one hour period in the lifetime of the cluster is considered. The rainfall amounts used here were therefore obtained by dividing Leary and Houze's values by 18.

The area of overhang of upper-level cloud surrounding the rain area of the cloud cluster (A_0 in Fig. 2b and Table 1) was not included in Leary and Houze's (1980) model since they were not concerned with the radiative transfer processes occurring there. The overhang has been added to their idealized cluster in this study by assuming that the total area of the cloud shield ($A_0+A_h+A_s$) is three times as large as the area covered by rain (A_h+A_s). This ratio was obtained by comparing the area of the satellite-observed cloud shield with the rain area of the 4-5 September 1974 GATE squall-line cloud cluster [studied by Houze (1977)] during its mature stage (from about 15 GMT on 4 September to 03 GMT on 5 September in Fig. 3). A cloud area to rain area ratio of 3 to 4 is generally representative of other clusters studied by the author, though in some cases the ratio can become greater.

Table 1 Properties of idealized cloud cluster and large-scale area containing it.

	Area Covered	Rainfall in 1 hr
Area of Convective Towers (A_h)	0.5×10^4 km^2	1.5×10^{11} kg
Stratiform Precipitation Area (A_s)	2.0×10^4 km^2	2.5×10^{11} kg
Upper-level Cloud Overhang (A_o)	7.5×10^4 km^2	0
Total area of Cloud Cluster ($A_h+A_s+A_o$)	10^5 km^2	4.0×10^{11} kg
Area of Large-scale Region containing Cloud Cluster (A)	2.0×10^5 km^2	4.0×10^{11} kg

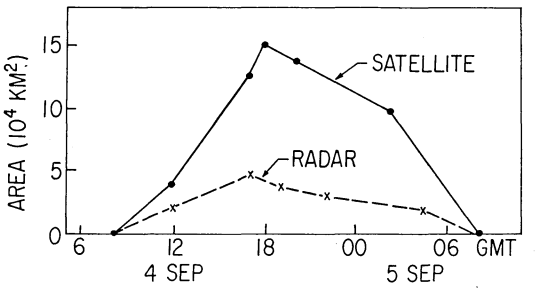

Fig. 3 Area covered by cirrus cloud shield, as shown by bright infrared satellite image, and area covered by precipitation, as shown by GATE radar data, for the squall-line cloud cluster observed over the GATE ship array on 4-5 September 1974. The cloud shield's boundary at times indicated by dots was taken to be the zone of strong infrared temperature gradient seen at the edge of the infrared feature associated with the precipitation area observed on radar. The precipitation areas for the times indicated by x's were determined from GATE radar data.

3. Formulation of the large-scale heat budget

The sensible heat budget of the large-scale region A containing the idealized cloud cluster described in Fig. 2 and Table 1 is formulated by first letting

$$A=A_c+A_e, \tag{1}$$

where A_c is the total area covered by cloud and A_e is the area of cloud-free environmental area surrounding the cluster. In the notation of Fig. 2, the area covered by cloud may be rewritten as

$$A_c=A_h+A_s+A_0 \tag{2}$$

where A_h is the area covered by hot towers, A_s the area covered by stratiform precipitation and A_0 the area covered by the cloud overhang. A_c is written in abbreviated form as

$$A_c=\sum_i A_i, \tag{3}$$

where i indicates the various subdivisions of the cloud area.

The sensible heat budget of area A is considered in terms of the dry static energy s, defined as the sum of the sensible heat and potential energy per unit mass. That is,

$$s=c_pT+gZ, \tag{4}$$

where c_p is the specific heat of dry air at constant pressure, T temperature, g the gravitational acceleration and z geopotential height.

The area-weighted average of a quantity ( ) is given by

$$\overline{(\ )}=\sigma_c(\ )_c+\sigma_e(\ )_e, \tag{5}$$

where σ_c and σ_e are the fractions of A covered by cloud and environment, and $(\ )_c$ and $(\ )_e$ are averages over the cloud and environment subregions, respectively. Application of (5) to the dry static energy and differentiation with respect to time lead to

$$\begin{aligned}\frac{\partial\bar{s}}{\partial t}&=\sigma_c\frac{\partial s_c}{\partial t}+\sigma_e\frac{\partial s_c}{\partial t}+s_c\frac{\partial\sigma_c}{\partial t}+s_e\frac{\partial\sigma_e}{\partial t}\\&=\sigma_cQ_{rc}+\sigma_eQ_{re}\\&\quad+\sigma_cL_v(c-e)+\sigma_cL_f(f-m)\\&\quad-\frac{1}{A}\oint V_nsdl\\&\quad-\frac{\partial}{\partial p}\left[\sum_i\omega_is_i\sigma_i+\omega_es_e\sigma_e\right]\\&\quad+\frac{\partial\sigma_c}{\partial t}(s_c-s_e)\end{aligned} \tag{6}$$

where Q_{rc} and Q_{re} are the net radiative heating in the cloud and environment regions, respectively, L_v the latent heat of vaporization, c condensation, e evaporation, L_f the latent heat of fusion, f freezing, m melting, p pressure, ω the vertical "p-velocity", and V_n the wind component normal to the boundary of A, around which the closed line integral is taken. The last term in (6) is obtained by noting that $\partial\sigma_e/\partial t=-\partial\sigma_c/\partial t$.

According to (3) and (5), the average vertical motion in region A is given by

$$\bar{\omega}=\sigma_e\omega_e+\sum_i\sigma_i\omega_i \tag{7}$$

Substitution of (7) into the term in brackets in (6) gives

$$\sum_i\omega_is_i\sigma_i+\omega_es_e\sigma_e=\sum_i\sigma_i\omega_is_i+s_e\left(\bar{\omega}-\sum_i\sigma_i\omega_i\right). \tag{8}$$

Substitution of (8) into (6) and rearrangement of terms leads to

$$\begin{aligned}\frac{\partial\bar{s}}{\partial t}+\frac{1}{A}\oint V_nsdl+\frac{\partial}{\partial p}(\bar{\omega}s_e)-\sigma_eQ_{re}\\=\sigma_cQ_{rc}+\sigma_cL_v(c-e)+\sigma_cL_f(f-m)\\-\frac{\partial}{\partial p}\sum_i\sigma_i\omega_i(s_i-s_e)\\+\frac{\partial\sigma_c}{\partial t}(s_c-s_e),\end{aligned} \tag{9}$$

where the terms on the right are associated with the cloud cluster. If no cloud cluster is present, all terms on the right are zero while those on the left remain.

In this paper, the terms on the right-hand side of (9) are estimated for the idealized cloud cluster described by Fig. 2 and Table 1. The sum of these terms gives the net heating by the cloud cluster, and this sum must be balanced by the terms on the left side of (9). In the tropics, vertical advection [*i.e.*, $\bar{\omega}(\partial s_e/\partial p)$] dominates the left-hand side for an area of the size assumed here for A.* Therefore, since $\partial s_e/\partial p$ is roughly constant in the troposphere of the tropics, the net heating obtained for the right-hand side of (9) may be interpreted as a direct indication of the mean (or large-scale) vertical motion $\bar{\omega}$ in area A.

This interpretation holds only for an area A that is not so large that the environmental radiation term on the left side of (9) becomes important. In one limiting case, A could be chosen large enough to cover the total region of the equatorial Hadley cell. In this extreme case, $\bar{\omega}$ and V_n and $\partial s/\partial t$ would be identically zero and the net heating of the cluster expressed by the

* This is seen by noting that conditions in the tropics are typically quite steady ($\partial\bar{s}/\partial t$ is small), radiative cooling in clear air ($\sigma_c\ Q_{re}$) is a slow process and that the other two terms on the right-hand side of (9) may be combined as follows:

$$\begin{aligned}&\frac{1}{A}\oint V_hsdl+\frac{\Delta(\bar{\omega}s_e)}{\Delta p}\\&=\frac{\Delta su}{\Delta x}+\frac{\Delta vs}{\Delta y}+\bar{\omega}\frac{\Delta s_e}{\Delta p}+s_e\frac{\Delta\bar{\omega}}{\Delta p}\\&=s\left(\frac{\Delta u}{\Delta x}+\frac{\Delta v}{\Delta y}\right)+u\frac{\Delta s}{\Delta x}+v\frac{\Delta s}{\Delta y}+\bar{\omega}\frac{\Delta s_e}{\Delta p}+s_e\frac{\Delta\bar{\omega}}{\Delta p}\\&\approx s_e\left(\frac{\Delta u}{\Delta x}+\frac{\Delta v}{\Delta y}\right)+\bar{\omega}\frac{\Delta s_e}{\Delta p}+s_e\frac{\Delta\bar{\omega}}{\Delta p}\\&=s_e\left(\frac{\Delta u}{\Delta x}+\frac{\Delta v}{\Delta y}+\frac{\Delta\bar{\omega}}{\Delta p}\right)+\bar{\omega}\frac{\Delta s_e}{\Delta p}\\&=\bar{\omega}\frac{\partial s_e}{\partial p}\end{aligned}$$

where Δx and Δy are the sides of area A and u and v are the horizontal wind components in the x and y directions, respectively. The last step is achieved by applying mass continuity. The approximation is obtained by noting that horizontal gradients of s (or T) are very slight in the tropics.

right-hand side of (9) would have to be balanced on the left-hand side by radiation rather than vertical advection of s. In this study, the area A is chosen to represent a much smaller area, *i.e.*, one in which the vertical advection dominates. The size of A assumed in Fig. 2 and Table 1 (2×10^5 km^2) corresponds physically to an area of synoptic-scale significance, for example, a subregion of an easterly wave, a portion of a tropical depression or a fixed region such as the main ship network in GATE.

4. Condensation and evaporation in the convective towers

The term for condensation minus evaporation in (9) may be written as

$$\sigma_c L_v(c-e)=\sigma_h L_v(c_{hu}-e_{hd}) + \sigma_s L_v(c_{mu}-e_{md}), \quad (10)$$

where σ_h is the fraction of A covered by the convective hot towers, c_{hu} is the condensation that occurs in updrafts of the towers, e_{hd} is the evaporation that occurs in the downdrafts of the towers, σ_s is the fraction of A covered by the stratiform precipitation of the cloud cluster, c_{mu} is the condensation that occurs in the mesoscale updraft of the stratiform region and e_{md} is the evaporation in the mesoscale downdraft.

In this section, the first term on the right of (10), containing the contributions of the convective updrafts and downdrafts is considered. The second term, involving the contributions of the mesoscale updraft and downdraft is discussed in Section 7.

The first term on the right of (10) is computed from the precipitation of the idealized cluster (Table 1) using the model of Leary and Houze (1980). According to their model, all the convective precipitation that falls in one hour (Table 1) is assumed to be produced by 14 km deep one-dimensional steady-state plumes with prescribed precipitation efficiency. Assumption of the efficiency allows the vertical mass transport in convective updrafts to be computed from the precipitation amount. Leary and Houze use an inverted plume model for the convective downdrafts, with an assumption being made about the fraction of total updraft condensate re-evaporated in the downdrafts. This assumption allows the vertical mass transport in convective downdrafts to be computed.

Leary and Houze considered three sets of assumptions (referred to in their paper as cases *A*, *B* and *C*) about the water budget of the idealized cloud cluster. Each set of assumptions included values for the convective precipitation efficiency and convective downdraft re-evaporation. In using Leary and Houze's results, their case *C*, which they considered to be the most realistic, is adopted. In that case, the convective precipitation efficiency (ratio of convective rainfall to convective condensation) was 48% and 13% of the updraft condensate was assumed to be re-evaporated in convective downdrafts.

In Leary and Houze's model, the entrainment rate for the 14 km plumes was assumed to be 0.01 km^{-1}. With this small entrainment rate, the hot towers are nearly undiluted.

The mass transports in convective updrafts and downdrafts computed by Leary and Houze (1980) were used here to calculate the convective updraft condensation c_{hu} and convective downdraft evaporation e_{hd} according to the relationships

$$c_{hu}=\left|\frac{\mu_{hu}}{\rho A_h}\frac{\partial q_{hu}}{\partial z}\right| \quad (11)$$

$$e_{hd}=\left|\frac{\mu_{hd}}{\rho A_h}\frac{\partial q_{hd}}{\partial z}\right| \quad (12)$$

where μ_{hu} and μ_{hd} are the masses of air transported vertically in convective updrafts and downdrafts, respectively, in a one-hour period, ρ is the density of the air, q_{hu} and q_{hd} are the mixing ratios of water vapor in the convective updrafts and downdrafts, respectively, and τ is one hour.

The mass transports μ_{hu} and μ_{hd} and mixing ratios q_{hu} and q_{hd} used in (11) and (12) were those computed by Leary and Houze (1980). The mass transports over an 18 h period computed by Leary and Houze were divided by 18 to obtain the values for a one hour period. The mixing ratios q_{hu} and q_{hd} were not shown in their paper, however, the records of the computations and computer programs used in that paper were still available and were used in obtaining the present results. For the density terms in (11) and (12), and elsewhere in the paper, a mean GATE sounding was used.

The condensation and evaporation in convective towers, c_{hu} and e_{hd}, obtained from (11) and (12), using Leary and Houze's (1980) values of μ_{hu}, μ_{hd}, q_{hu}, and q_{hd}, are multiplied by the factor $L_v\sigma_h$ and given appropriate signs to obtain the first term on the right-hand side of (10), which expresses the contributions of the convective updraft condensation and downdraft evaporation to the net heating and cooling over area

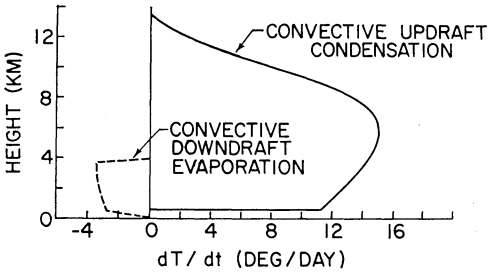

Fig. 4 Heating of large-scale area A by condensation in the updrafts and cooling by evaporation in the downdrafts of convective towers in the idealized cloud cluster.

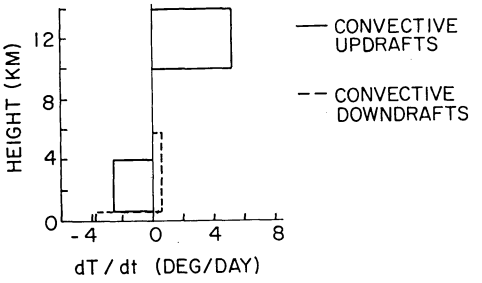

Fig. 5 Heating and cooling of large-scale area A owing to the convergence of sensible heat flux by the updrafts and downdrafts of the convective towers in the idealized cloud cluster.

A. These heating and cooling rates are plotted in Fig. 4 in units of °C/day. These units are obtained by dividing the terms in (10) by c_p. The results show strong heating through the full depth of the troposphere as a result of condensation in the convective updrafts. This heating is partially offset in the lower troposphere by evaporative cooling in the convective downdrafts.

5. Convergence of sensible heat flux in convective cells

The term for the vertical convergence of sensible heat flux associated with cloud updrafts and downdrafts in (9) may be written as

$$-\frac{\partial}{\partial p}\sum_i \sigma_i\omega_i(s_i-s_e)=-\frac{\partial}{\partial p}[\sigma_h\omega_{hu}(s_{hu}-s_e) + \sigma_h\omega_{hd}(s_{hd}-s_e)+\sigma_m\omega_m(s_m-s_e)], \quad (13)$$

where hu, hd and m refer to convective updrafts, convective downdrafts and mesoscale drafts. The first two terms in the brackets in (13), which express the sensible heat fluxes associated with the updrafts and downdrafts of convective towers, are considered in this section. The term expressing the contribution of the mesoscale drafts is discussed in Section 8.

The static energies s_{hu} and s_{hd} and vertical motion ω_{hu} and ω_{hd} appearing in the convective terms of (13) are obtained from the calculations of Leary and Houze (1980), the vertical motions being given by

$$\omega_{hu}=-g\frac{\mu_{hu}}{A_h\tau} \quad (14)$$

and

$$\omega_{hd}=-g\frac{\mu_{hu}}{A_h\tau}. \quad (15)$$

The first two terms on the right-hand side of (13), expressed in °C/day by dividing them by c_p, are plotted in Fig. 5. The convergence of heat flux by the convective updrafts cools the lower troposphere and warms the upper troposphere. The downdrafts have only a slight effect, except near the surface.

6. Total heating by convective towers

When the heating and cooling by convective updraft condensation and convective downdraft evaporation (Fig. 4) are added to the convergence of heat flux in convective updrafts and downdrafts (Fig. 5), the total heating of the large-scale area A by convective cells is obtained (Fig. 6). The result is heating, dominated by the condensation in convective updrafts extending through the whole depth of the troposphere. If the upper-level cloud shield of the cluster was passive, the convective cells would be the only phenomena contributing to the cloud cluster's heating of the large-scale area A, and Fig. 6 would be the total heating function. The upper-

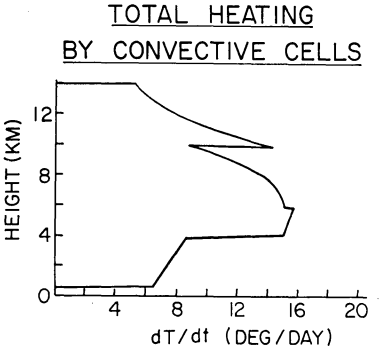

Fig. 6 Total heating of large-scale area A by the convective towers in the idealized cloud cluster. The curve is obtained by adding the curves in Figs. 4 and 5.

level cloud shield, however, is not passive, and the next sections of the paper are concerned with the contributions of its mesoscale and radiative processes to the total heating function of the cluster.

7. Heating and cooling associated with phase changes in the stratiform precipitation region of the cluster

In the stratiform precipitation region of the cluster, condensation occurs in the mesoscale updraft aloft, melting takes place near cloud base and evaporation occurs in the mesoscale downdraft below cloud base (Fig. 2b). The heating and cooling of air associated with these phase changes are included in the terms $\sigma_c L_v (c\text{-}e)$ and $\sigma_c L_f (f\text{-}m)$ in Eq. (9).

The term involving the latent heat of vaporization $[\sigma_c L_v (c\text{-}e)]$, was re-expressed by Eq. (10), where it is seen to consist of contributions by both the convective and mesoscale updrafts and downdrafts of the cloud cluster. The convective updraft and downdraft contributions were considered in Section 4 and plotted in Fig. 4. The heating by condensation in mesoscale updrafts ($\sigma_s L_v c_{mu}$) and cooling by evaporation in mesoscale downdrafts ($-\sigma_s L_v e_{md}$) are considered in this section.

The latent heat of fusion term $[\sigma_c L_f (f\text{-}m)]$ is also considered here. It is assumed to be given by

$$\sigma_c L_f (f-m) = -\sigma_s L_f m. \tag{16}$$

That is, the melting in the stratiform precipitation region is assumed to be the only important contribution to this term.

To estimate the mesoscale stratiform latent heat terms $\sigma_s L_v c_{mu}$, $-\sigma_s L_v e_{md}$ and $-\sigma_s L_f m$, reference is made to papers by Leary and Houze (1979b, 1980). In the 1980 paper, the mesoscale updraft and downdraft transports were determined from the precipitation amounts of the idealized cluster using simple models of the updraft and downdraft motions in the stratiform region and assumptions about the water budget of the cluster. As in Section 4, their case *C* water budget assumptions are adopted in obtaining results for this paper. The mesoscale updraft condensation and downdraft evaporation were obtained from Leary and Houze's (1980) results using the relationships

$$c_{mu} = \left| \frac{\mu_{mu}}{\rho A_s \tau} \frac{\partial q_{mu}}{\partial z} \right| \tag{17}$$

and

$$e_{md} = \left| \frac{\mu_{md}}{\rho A_s \tau} \frac{\partial q_{md}}{\partial z} \right| \tag{18}$$

where μ_{mu} and μ_{md} are the masses of air transported vertically in the mesoscale updraft and downdraft, respectively, in a one-hour period, and q_{mu} and q_{md} are the mixing ratios of water vapor in the mesoscale updraft and downdraft, respectively. The quantities μ_{mu}, μ_{md}, q_{mu} and q_{md} were all obtained from the records and computer programs used in the study of Leary and Houze (1980).

The heating by condensation in the mesoscale updraft ($\sigma_s L_v c_{mu}/c_p$), obtained with c_{mu} computed according to (17) and Leary and Houze's (1980) model, is shown in the upper part of Fig. 7. The cooling by evaporation in the mesoscale downdraft ($-\sigma_s L_v e_{md}/c_p$), obtained with e_{md} computed according to (18) using Leary and Houze's (1980) model, had an average value of -5.7°C/day through the depth of the layer containing the downdraft. In the paper of Leary and Houze (1979b), the evaporational cooling rates in the lower troposphere of the stratiform precipitation regions of five cloud clusters were calculated from vertical profiles of radar reflectivity. The mean value for the five cases (when applied over large-scale area *A*) was -5.3°C/day. This result agrees well with the model result (-5.7°C/day), and a value of -5.5°C/day, the mean of the two estimates, is plotted in Fig. 7 in the layer containing the mesoscale downdraft.

Leary and Houze (1979b) also used vertical profiles of radar reflectivity to estimate cooling in the melting layers of the stratiform regions of their five clusters. The melting layers were located between 3.3 and 4.5 km, on average, and the

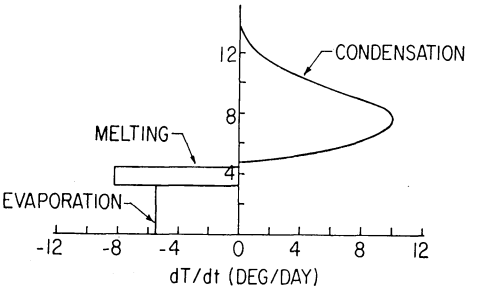

Fig. 7 Heating of large-scale area *A* by condensation in the mesoscale updraft, cooling by evaporation in the mesoscale downdraft and cooling by the melting of precipitation particles in the stratiform precipitation region of the idealized cloud cluster.

mean cooling rate in this layer (when applied over A) was -8.2°C/day. This value is shown for the cooling associated with melting of stratiform precipitation ($-\sigma_s L_f m/c_p$) in Fig. 7.

8. Convergence of sensible heat flux in the stratiform region

The contributions of mesoscale air motions in the stratiform precipitation region of the cloud cluster to the convergence of sensible heat flux over area A is given by the last term in (13), which may be rewritten as

$$-\frac{\partial}{\partial p}[\sigma_m \omega_m (s_m - s_e)] = \begin{cases} -\dfrac{\partial}{\partial p}[\sigma_m \omega_{mu}(s_{mu} - s_e)], & z > z_m \\ -\dfrac{\partial}{\partial p}[\sigma_m \omega_{md}(s_{md} - s_e)], & z \leqq z_m \end{cases} \tag{19}$$

where mu and md refer to the mesoscale updraft and downdraft, respectively, and z_m is the height of cloud base in the stratiform precipitation area (Fig. 2b).

The static energies s_{mu} and s_{md} and vertical motions ω_{mu} and ω_{md} are obtained from Leary and Houze's (1980) calculations, the vertical motions being given by

$$\omega_{mu} = -g\frac{\mu_{mu}}{A_s \tau} \tag{20}$$

and

$$\omega_{md} = -g\frac{\mu_{md}}{A_s \tau}. \tag{21}$$

The convergence of sensible heat flux given by (19) is divided by c_p to express results in °C/day. The profile obtained is shown in Fig. 8, with the contributions of the mesoscale updraft and downdraft indicated. The magnitude of this term can be seen to be small in comparison to the mesoscale latent heat effects plotted in Fig. 7.

9. Total heating by non-radiative processes in the stratiform region

The thermodynamic processes in the stratiform region of the cloud cluster include the heating and cooling associated with latent heat release, *i.e.*, condensation, evaporation and melting (Fig. 7), the convergence of sensible heat flux by the mesoscale updraft and downdraft (Fig. 8) and radiative emission and absorption. Radiation is considered in Section 10. The total heating of the large-scale area A by non-radiative processes in the stratiform precipitation region is obtained by adding the profiles in Figs. 7 and 8. The result is shown as Fig. 9. Strong heating, dominated by condensation in the mesoscale updraft, occurs above 5 km. The lower levels are dominated by cooling associated with melting between 3.3 and 4.5 km and evaporation in the mesoscale downdraft below 3.3 km.

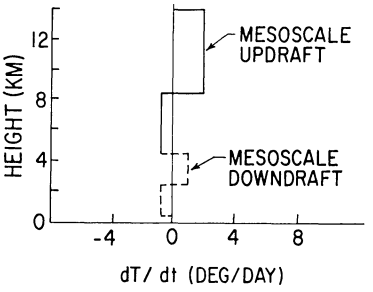

Fig. 8 Heating and cooling of large-scale area A by the convergence of sensible heat flux by the mesoscale updraft and mesoscale downdraft in the stratiform precipitation region of the idealized cloud cluster.

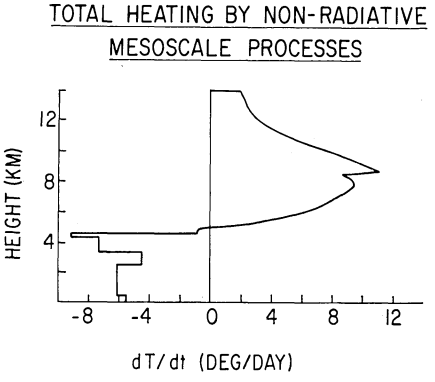

Fig. 9 Total heating and cooling of large-scale area A by non-radiative processes in the stratiform precipitation region of the idealized cluster. The curve is obtained by adding the curves in Figs. 7 and 8.

10. Radiative heating in the cloud cluster

The contribution of net radiative absorption and emission to the sensible heat budget of region A is expressed by the term $\sigma_c Q_{rc}$ in Eq. (9). This term may be written as

$$\sigma_c Q_{rc} = (\sigma_h + \sigma_s) Q_{rb} + \sigma_0 Q_{ra}, \tag{22}$$

where $(\sigma_h + \sigma_s)$ is the fraction of area A covered by precipitation [that is, the fraction of A covered by hot towers (A_h) and stratiform precipitation areas (A_S); see Fig. 2b], σ_0 is the fraction of A covered by the overhang of upper-level cloud surrounding the precipitation area (A_0 in Fig.

2b), and Q_{rb} and Q_{ra} are the net radiative heating rates in the areas of precipitation and overhang, respectively.

Values for Q_{rb} and Q_{ra} were obtained from Figs. 9b and 9a, respectively, of Webster and Stephens (1980). Their values were computed with the model of Stephens (1978) for the upper cloud shields of tropical cloud clusters. Their Fig. 9b was for a cloud shield in a layer between 4.4 and 12.3 km (600 and 200 mb), while their Fig. 9a was for a cloud lying between 8.5 and 12.3 km (350 and 200 mb). The results for the deeper cloud (their Fig. 9b) were used for the radiative heating in the precipitation area Q_{rb}, while their results for the shallower cloud (their Fig. 9a) were used for Q_{ra}. The profiles taken from Webster and Stephens' (1980) Figs. 9a and b were their total terrestrial plus solar heating, corresponding to daytime conditions.

The values for radiative heating in the precipitation area $[(\sigma_h+\sigma_s)Q_{rb}/c_p]$ and the overhang $[\sigma_0 Q_{ra}/c_p]$ obtained using Webster and Stephens' (1980) results are shown in Fig. 10. The total heating obtained by adding the profiles in Fig. 10 is shown in Fig. 11. The result is net heating in the middle to upper troposphere, with the strongest contribution near cloud top.

The heating rates seen in Fig. 11 are significant, though not as great as those associated with condensation, evaporation and melting (*cf.*, Figs. 4 and 7).

The importance of the radiative heating in cloud clusters is actually greater than may be evident from comparing Figs. 4, 7 and 11. Its importance is more subtle in at least four respects:

(i) The idealized cloud cluster considered in this study has rather high rainfall rates and correspondingly large vertical air motions and latent heat effects. Real cloud clusters may frequently develop cloud shields as large as in the idealized case but not have as much rainfall. Webster and Stephens (1980) point out that in such cases the radiative heating is probably just as strong as in heavy rainfall cases and thus takes on more importance relative to the latent heating and cooling mechanisms.

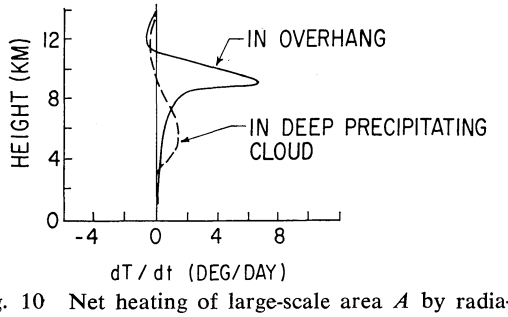

Fig. 10 Net heating of large-scale area A by radiative absorption and emission in cloud overhang (Area A_o) and in the precipitation region (area A_h+A_s) of the idealized cloud cluster. Profiles are for daytime conditions and are adapted from Webster and Stephens (1980).

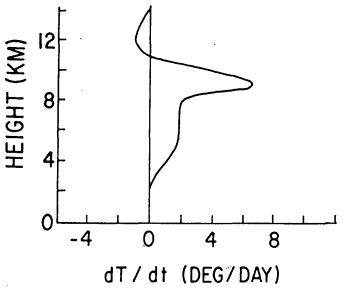

Fig. 11 Total heating of large-scale area A by radiative processes in the idealized cloud cluster. The curve is obtained by adding the two curves in Fig. 10.

(ii) Calculations in this study have been made for the mature stage of a cluster, that is, when it contains very active latent heating and cooling processes. As the precipitation and vertical air motions weaken and die, the upper-level cloud shield remains for a long time absorbing and emitting radiation. Therefore, when heating and cooling processes are integrated over the lifetime of the cluster, radiation takes on more importance in relation to the other processes.

(iii) Calculations have been made here for daytime conditions only. As shown by Cox and Griffith (1979) and Webster and Stephens (1980) the radiative heating in a cluster varies strongly with the daily cycle of insolation. Diurnal variability in the activity of cloud clusters and their heating effects is therefore expected and, in fact, observed throughout the tropics, including open ocean areas, far from land masses where land-sea breeze effects account for the diurnal variability (Gray and Jacobson, 1977; Short and Wallace, 1980; McBride and Gray, 1980; Albright *et al.*, 1981).

(iv) The radiative heating reinforces the other heating processes associated with the cluster. This point is discussed in Section 12.

11. Expansion and contraction of the cloud cluster

The last term in (9), $(\partial\sigma_c/\partial t)(s_c-s_e)$, expresses

the rate at which the average value of static energy in area A increases or decreases as a result of the cluster increasing or decreasing in size. This term can be estimated by noting that the area of the idealized cluster during its mature stage (Fig. 2b) covers one-half of A. If it takes one-fourth to one-half a day to reach this size, and if the mean temperature difference between the area covered by the cluster and the environment is $\leq 1°C$, then $c_p^{-1}(\partial \sigma_c / \partial t)\,|s_c - s_e|$ has a value of, at most, 1-2°C/day, which is small compared to the latent heat and radiation terms on the right-hand side of (10) (*cf.*, Figs. 4, 7, and 11). Therefore, this term is neglected in the remainder of this paper.

12. Total heating by the cloud cluster and response on the large scale

The total heating of the large-scale area A by the cloud cluster is obtained by summation of the profiles in Figs. 6, 9 and 11. The result is the solid curve in Fig. 12. This curve gives the sum of the terms on the right-hand side of (a) (after the terms have been divided by c_p to give units of °C/day and the area-change term, discussed in Section 11, is neglected). The heating associated with the convective towers alone (taken from Fig. 6) is shown for comparison by the dashed curve in Fig. 12.

The heating profiles in Figs. 6, 9 and 11 are all positive above 5 km, with largest values between 5 and 10 km. Therefore, the profiles reinforce each other in the middle to upper troposphere, with the result that the total heating of the cluster, including its mesoscale stratiform (Fig. 9) and radiative (Fig. 11) components, as well as its convective towers (Fig. 6), is much stronger than the heating owing to the convective towers alone in middle to upper levels (compare the solid and dashed curves in Fig. 12 above 5 km).

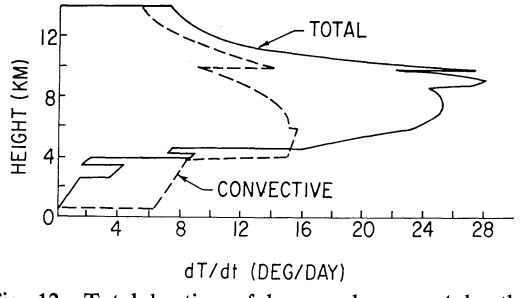

Fig. 12 Total heating of large-scale area A by the idealized mature cloud cluster (solid curve). The total heating by the convective towers alone (dashed curve) is shown for comparison.

At lower levels, cooling by evaporation and melting in the stratiform precipitation region of the cluster is significant (*cf.*, the negative values below 5 km in Fig. 9). This cooling tends to cancel the heating by convective towers (Fig. 6), and the total heating at lower levels in the cluster is, therefore, less than that associated with the convective towers alone (*i.e.*, the solid curve lies to the left of the dashed curve below 5 km in Fig. 12).

The reinforcement of the various heating processes in the cluster in middle to upper levels has important implications. It means that the cluster has no mechanism for counteracting its own heating at these levels. The terms on the right-hand side of (9), therefore, sum to a large positive number, which must be balanced by the large-scale terms on the left. Since, as noted at the end of Section 3, the only significant large-scale term on the left is the vertical advection $\bar{\omega}(\partial s_e / \partial p)$, and since $\partial s_e / \partial p$ is negative, large-scale upward motion ($\bar{\omega} < 0$) must occur in the middle to upper troposphere to balance the heating associated with the cluster at these levels.

The lack of reinforcement associated with the opposing effects of the various heating and cooling processes at lower levels in the cluster also has important implications. Since the heating associated with convective towers tends to be cancelled by the cooling effects of mesoscale stratiform evaporation and melting, the terms on the right-hand side of (9) sum to a small number, with the result that little large-scale vertical motion is required in the advection term on the left. Thus, the presence of a mature cloud cluster requires strong large-scale motion in middle to upper levels but little large-scale response at lower levels.

13. Changes in heating and large-scale response as a cluster develops

In its beginning stages, a cloud cluster is purely convective, containing only hot towers (Fig. 2a). It is only after it reaches maturity that it contains a widespread cloud shield, with important mesoscale stratiform precipitation processes and radiative effects (Fig. 2b). It takes some 6-12 h to reach maturity. Therefore, the two curves in Fig. 12 can be interpreted as the heating function of the cluster at two stages of its life cycle. The convective curve represents an early stage, when the convective towers are intense but before

the upper-level cloud shield develops, while the total curve represents the mature stage of the cluster.

With this interpretation, the two curves in Fig. 12 indicate that the heating function of the cluster [*i.e.*, the sum of the terms of the right-hand side of (9)] varies strongly with time during the evolution of the system. This variation must, in turn, be reflected in the large-scale vertical motion term, which dominates the left-hand side of (9). The profile of $-\bar{\omega}$, in fact, should change in the same sense as the heating profiles in Fig. 12 over the developing stage of a cluster, since the vertical advection is directly proportional to the total heating by the cloud cluster.

Analysis of upper-air data from the *A/B*-scale ship network in GATE supports this conclusion. Figs. 13-15 are from case studies in which cloud clusters were within the GATE sounding network. The earlier times shown are for the developmental stages of the clusters, while the later times are for the clusters' middle or later stages of development. In each figure, the vertical motion $(-\bar{\omega})$ is seen to have decreased at low levels and increased aloft as clusters matured.

Perhaps more convincing than the case-study results are statistical composites of the GATE upper-air data. Frank (1978) constructed composites according to the stage of development of cloud clusters in the GATE *A/B*-scale array (Fig. 16). Stage 3 represents the early stage and Stage 5 the mature stage. Albright *et al.*, (1981) derived composites for various times of day (Fig. 17). At 0230 LST, the convection in the GATE array tended to be just developing, by 1500 LST mature clusters tended to be formed and by 1800 LST cloud systems in the array were weak-

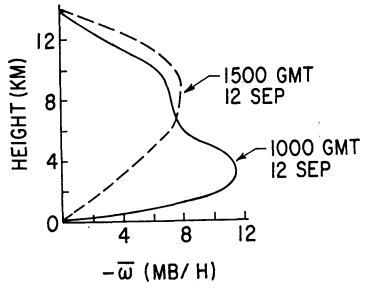

Fig. 13 Average vertical motion $(-\bar{\omega})$ in the GATE A/B-scale ship network on 12 September 1974. From Nitta (1977).

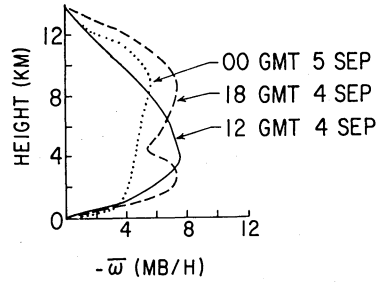

Fig. 14 Average vertical motion $(-\bar{\omega})$ in the GATE A/A-scale ship network on 4-5 September 1974. From Ogura *et al.* (1979).

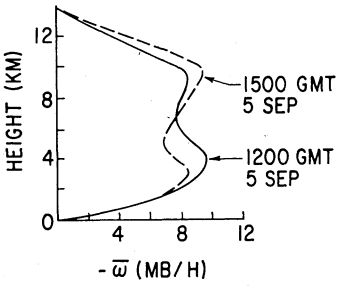

Fig. 15 Average vertical motion $(-\bar{\omega})$ in the GATE A/B-scale ship array on 5 September 1974. From Ogura *et al.* (1979).

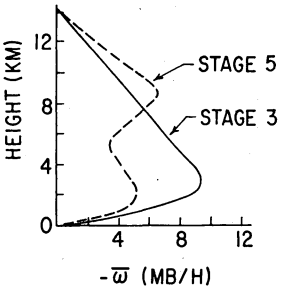

Fig. 16 Composite of average vertical motion in the GATE A/B-scale ship network for periods when cloud clusters in the array are just developing (Stage 3) and mature (Stage 5). From Frank (1978).

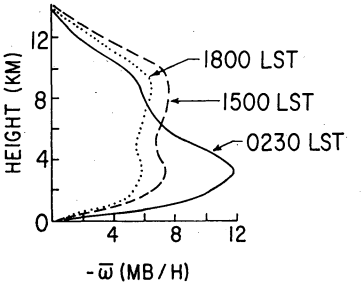

Fig. 17 Composite of average vertical motion in the GATE A/B-scale ship network for different times of day. From Albright *et al.* (1978).

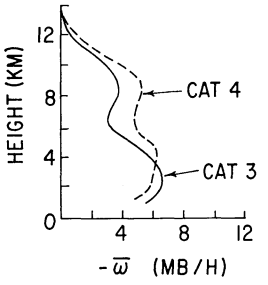

Fig. 18 Composite of average vertical motion in the GATE A/B-scale ship network for regions just ahead of the troughs (CAT. 3) and in the troughs (CAT. 4) of synoptic-scale easterly waves. From Thompson *et al.* (1979).

ening. Thompson *et al.* (1979) constructed composites for various portions of easterly waves passing over the GATE ship network (Fig. 18). Category 3 represents the region just ahead of wave troughs where convection tended to be in early stages of development, while Category 4 is the wave-trough region, where more mature cloud clusters typically were found. In each of these composite studies, the value of $-\bar{\omega}$ increased at upper levels and decreased at lower levels as the cloud systems in the GATE array proceeded from early to later stages of development.

14. Conclusions

Deep convection in the equatorial tropics involves more than cumulus-scale "hot towers." The upper-level cloud shields of mesoscale cloud clusters, within which the towers are usually embedded, are also dynamically and thermodynamically active. The cloud shields contain mesoscale stratiform precipitation regions, where condensation occurs in a mesoscale updraft aloft, evaporation occurs in a mesoscale downdraft at low levels and melting occurs in a middle-level layer. Radiative heating is important throughout the widespread cloud shield. The mesoscale stratiform precipitation processes and radiation combine with the convective towers to give the total heating of a mature cloud cluster.

A cloud cluster proceeds through a life cycle, in which it first consists only of convective towers. Later in its lifetime, it develops a widespread cloud shield, in which mesoscale updraft condensation and radiation add substantially to the convective-tower heating at levels above 5 km, especially between 5 and 10 km. Thus, the total heating associated with the cluster in middle to upper levels increases as the cluster matures. Cooling associated with melting and evaporation of stratiform precipitation falling from the cloud shield, on the other hand, cancels much of the convective heating at levels below 5 km. Thus, the total heating associated with the cluster decreases at lower levels as the cluster matures. The increase in heating aloft and decrease at low levels that occurs as the cluster matures must be accompanied by an increase in large scale upward motion ($-\bar{\omega}$) aloft and a decrease at low levels, since the vertical advection of dry static energy by $\bar{\omega}$ must nearly balance the heating associated with the cluster. Observations of large-scale vertical motions in GATE confirm that $-\bar{\omega}$ increased at upper levels and decreased at lower levels as cloud clusters in the observational network progressed from early to mature stages of development.

This study thus shows that the mesoscale stratiform and radiative processes associated with the cloud shields of tropical cloud clusters modify vertical profiles of heating sufficiently strongly during the development of clusters to alter the large-scale vertical motion field. This significant interaction of processes on the scale of the cluster's cloud shield with larger scales of motion in the tropics was not generally recognized prior to GATE and MONEX. However, the data and descriptions of cloud clusters now available from these field programs have made studies such as the present one possible and, as a result, it is now clear that the cloud shield of a cluster defines an active region, which must be reckoned with in tropical dynamics.

Acknowledgements

This paper was presented at the Third Scientific Assembly of the International Association of Meteorology and Atmospheric Physics, Hamburg, 17-28 August 1981, at the invitation of Dr. Peter J. Webster, convenor of the Assembly's symposium on tropical meteorology. Prof. Colleen A. Leary and Dr. Chee-Pong Cheng provided information crucial to the calculations, and Prof. Richard J. Reed made helpful comments. This paper is Contribution Number 609, Department of Atmospheric Sciences, University of Washington. The research was sponsored by the Global Atmospheric Research Program, National Science Foundation, and the GATE Project Office, National Oceanic and Atmospheric Administration, under Grants ATM78-16859 and ATM80-17327.

References

Albright, M. D., D. R. Mock, E. E. Recker, and R. J. Reed, 1981: A diagnostic study of the diurnal rainfall variation in the GATE B-scale area. *J. Atmos. Sci.*, **38**, 1429-1435.

Brown, J. M., 1979: Mesoscale unsaturated downdrafts driven by rainfall evaporation: A numerical study. *J. Atmos. Sci.*, **36**, 313-338.

Cox, S. K., and K. T. Griffith, 1979: Estimates of radiative divergence during Phase III of the GARP Atlantic Tropical Experiment: Part II. Analysis of the Phase III results. *J. Atmos. Sci.*, **36**, 568-601.

Frank, N. L., 1970: Atlantic tropical systems of 1969. *Mon. Wea. Rev.*, **98**, 307-314.

Frank, W. M., 1978: The life cycles of GATE convective systems. *J. Atmos. Sci.*, **35**, 1256-1264.

Gamache, J. F., and R. A. Houze, Jr., 1982: Mesoscale air motions associated with a tropical squall line. *Mon. Wea. Rev.* In press.

Gray, W. M., and R. W. Jacobson, Jr., 1977: Diurnal variation of oceanic deep cumulus convection. *Mon. Wea. Rev.*, **105**, 1171-1188.

Houze, R. A., Jr., 1977: Structure and dynamics of a tropical squall-line system observed during GATE. *Mon. Wea. Rev.*, **105**, 1540-1567.

————, and A. K. Betts, 1981: Convection in GATE. *Reviews of Geophysics and Space Physics*, **19**, 541-576.

Leary, C. A., and R. A. Houze, Jr., 1979a: The structure and evolution of convection in a tropical cloud cluster. *J. Atmos. Sci.*, **36**, 437-457.

————, and ————, 1979b: Melting and evaporation of hydrometeors in precipitation from the anvil clouds of deep tropical convection. *J. Atmos. Sci.*, **37**, 784-796.

————, and ————, 1980: The contribution of mesoscale motions to the mass and heat fluxes of an intense tropical convective system. *J. Atmos. Sci.*, **37**, 784-796.

Martin, D. W., and O. Karst, 1969: A census of cloud systems over the tropical Pacific. Studies in Atmospheric Energetics Based on Aerospace Probings, Ann. Rept., 1968, Space Science and Engineering Center, Univ. of Wisconsin.

————, and V. E. Suomi, 1972: A satellite study of cloud clusters over the tropical North Atlantic Ocean. *Bull. Amer. Meteor. Soc.*, **53**, 135-156.

McBride, J. L., and W. M. Gray, 1980: Mass divergence in tropical weather systems, Paper I: Diurnal variations. *Quart. J. Roy. Meteor. Soc.*, **106**, 501-516.

Nitta, T., 1977: Response of cumulus updraft and downdraft to GATE A/B-scale systems. *J. Atmos. Sci.*, **34**, 1163-1186.

Ogura, Y., M.-T. Liou, J. Russell, and S. T. Soong, 1979: On the formation of organized convective systems observed over the eastern Atlantic. *Mon. Wea. Rev.*, **107**, 426-441.

Riehl, J., and J. S. Malkus, 1958: On the heat balance in the equatorial trough zone. *Geophysica*, **6**, 503-538.

Riehl, H., and J. Simpson, 1979: The heat balance of the equatorial trough zone, revisited. *Beitr. Phys. Atmosph.*, **52**, 287-305.

Short, D. A., and J. M. Wallace, 1980: Satellite-inferred morning-to-evening cloudiness changes. *Mon. Wea. Rev.*, **108**, 1160-1169.

Stephens, G. L., 1978: Radiative properties of extended water clouds, Part I. *J. Atmos. Sci.*, **35**, 2111-2122.

Thompson, R. M., Jr., S. W. Payne, E. E. Recker and R. J. Reed, 1979: Structure and properties of synoptic-scale wave disturbances in the intertropical convergence zone of the eastern Atlantic. *J. Atmos. Sci.*, **36**, 53-72.

Webster, P. J., and G. L. Stephens, 1980: Tropical upper-tropospheric extended clouds: Inferences from Winter MONEX. *J. Atmos. Sci.*, **37**, 1521-1541.

Zipser, E. J., 1969: The role of organized unsaturated downdrafts in the structure and rapid decay of an equatorial disturbance. *J. Appl. Meteor.*, **8**, 799-814.

熱帯の雲クラスターと大規模上昇流

Robert A. Hauze, Jr.

Department of Atmospheric Sciences, University of Washington

雲クラスターを含む熱帯大規模場の熱収支解析を行った。クラスターの大きさと降水量は観測から得られた平均的な値を用いた。

モデル化されたクラスターは発達の初期には，孤立した背の高い，降水を伴なう対流セルから成立っている。降水率を仮定した簡単な雲モデルを用いて，対流雲の凝結熱，蒸発率，顕熱輸送量を求めた。対流雲が大規模場の熱収支に与える影響では凝結熱放出が主要な役割を果し，対流雲は全体として対流圏全層を暖めている。

発達の最盛期では，クラスターは対流雲と横に広く拡がる雲のおおいを含んでいる。この広く雲でおおわれた

領域では力学的にも熱力学的にも活発で，大規模場の熱収支に大きな役割を果している。またこの領域では雨が降っており，上層のメソスケールの上昇域では凝結が，下層の下降域では蒸発がおこっており，その中間で氷解がおこっている。メソスケールの上昇域，下降域での凝結熱，蒸発熱，顕熱輸送量は，降水率を仮定した簡単なモデルで決定される。また氷解熱は実際の雲クラスターでのレーダ観測による反射率から見積られる。雲の広くおおっている領域では全体として中層から上層では熱源，下層では冷源の役割を果している。

この雲でおおわれた領域はまた放射エネルギーにとっても重要である。この領域では中層から上層にかけて放射によって温められており，この効果は他の凝結熱や蒸発熱と同程度に重要な役割を果している。

雲クラスターの発達段階によって，大規模熱収支に及ぼす影響は変化している。水平に雲のおおう領域が拡大するにつれ，上層ではメソ上昇域の凝結熱と放射効果によってより熱せられ，下層のメソ下降域では蒸発によって冷やされる。従ってクラスターが発達するにつれ上層では加熱率が増大し，下層では逆に減少する。これらの結果は観測から得られた大規模上昇速度の分布とよく対応している。以上のことから，発達した雲クラスターでは，雲で広くおおわれた領域におけるメソスケールの上昇，下降運動，および放射加熱の効果が大きく，熱帯の大規模上昇流に重要な影響を与えるということが結論される。